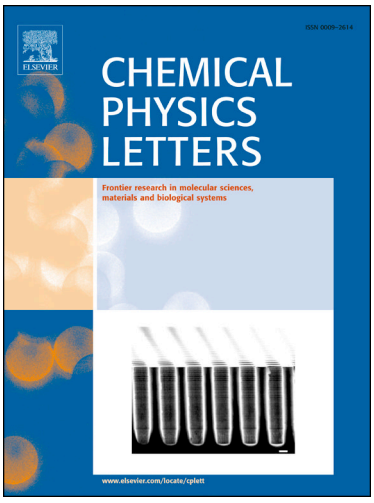

Reactivity of Cycloparaphenylenes: Studying the Possible Growth of Single-walled Carbon Nanotubes with DFT methods

M. Reche-Tamayo, A. Pérez-Guardiola, A.J. Pérez-Jiménez, J.C. Sancho-García

PII: S0009-2614(18)30101-5
DOI: https://doi.org/10.1016/j.cplett.2018.02.017
Reference: CPLETT 35429

To appear in: *Chemical Physics Letters*

Received Date: 13 December 2017
Accepted Date: 7 February 2018

Please cite this article as: M. Reche-Tamayo, A. Pérez-Guardiola, A.J. Pérez-Jiménez, J.C. Sancho-García, Reactivity of Cycloparaphenylenes: Studying the Possible Growth of Single-walled Carbon Nanotubes with DFT methods, *Chemical Physics Letters* (2018), doi: https://doi.org/10.1016/j.cplett.2018.02.017

Reactivity of Cycloparaphenylenes: Studying the Possible Growth of Single-walled Carbon Nanotubes with DFT methods

M. Reche-Tamayo, A. Pérez-Guardiola,
A. J. Pérez-Jiménez, and J. C. Sancho-García*

Department of Physical Chemistry,
University of Alicante, E-03080 Alicante, Spain

February 5, 2018

*E-mail: jc.sancho@ua.es

Abstract

We perform a theoretical study on a set of carbon nanorings (CycloParaPhenylenes or CPP) envisioned as molecular templates for the selective synthesis of carbon nanotubes. The shape of these precursors, originating from bending n phenylene units in *para* position until forming the corresponding nanoring [n]CPP, may drive the growth of armchair single-walled nanotubes. This kinetic and thermodynamic study covers a set of molecules with different diameters, analyzing the exothermicity and the reaction path of a CPP-based radicaloid mechanism. The methodology employed is based on validated density functionals for mechanistic studies, shedding light on the viability of this synthetic pathway.

Key words: CycloParaPhenylenes, SWCNT, chemical reactivity, thermochemical kinetics, density functionals.

1 Introduction

Nanotechnology is a challenging and growing field of knowledge that has aroused a big interest in the scientific community along the last years; one of the outstanding advances in this field are Carbon NanoTubes (CNTs), and the development of this technology has been one of the main worldwide goals in last decades. Currently, CNTs comprise a wide range of usage, from raw application in industry to more sophisticated ones in the lithium-ion batteries.[1] More specific investigations are devoted to disclose new (clean and selective) synthetic ways, envisioning more sophisticated applications (e.g. for organic electronic applications) and overcoming the traditional synthesis based on arc-discharge,[2] laser ablation[3] or chemical vapor deposition,[4] to name just a few of them. Interestingly, the use of molecular templates as chemical precursors is an emergent and relatively novel strategy from the synthetic point of view, ideally affording the size-specific growth of CNTs. This technique is based on employing n-ring CycloParaPhenylene ([n]CPP, see Figure 1) molecules as adequate substrates for the spontaneous self-assembly and growth of the corresponding armchair CNT under certain reaction conditions,[5,6] thanks to progress in epitaxial growth of Single-Walled (SW) CNTs.[7] Note that the design and bottom-up synthesis of CNT segments has progressed enormously along last years,[6,8,9] and that synthesis of chiral or zig-zag CNTs could be also accomplished using other cyclic nanorings as precursors, although these other routes will not be studied here.

Only very recently some experimental evidences for the specific synthesis of SWCNT following this strategy were presented,[10] after treatment of [12]CPP spin-coated on a C-plane saphire substrate with a flow of ethanol gas at high temperatures. The histograms with the CNT diameters distribu-

tion showed pronounced peaks consistent with the diameter ($1.5 - 1.6$ nm) of the [12]CPP used as a precursor,[11] confirming TEM images and thus the successful synthesis. The authors comprehensively revised the two main possible reaction mechanisms proposed so far for CPP-initiated CNT growth, namely: (i) a neutral and classical Diels-Alder mechanism involving [n]CPP and acetylene C_2H_2, as diene and dienophile respectively, studied before in this context by Scott *et al.*;[12] and (ii) the ethynyl ($C_2H\cdot$) radical addition mechanism, which is formed *in situ* from C_2H_2, also studied extensively before by Morokuma *et al.*[13,14] Importantly, the authors did not experimentally observe any production of CNTs using $C_2H\cdot$ or C_2H_2 as reactive agents, but the intrinsically entangled reaction conditions (i.e. temperature, reaction plate, and carbon source) did not allow to clearly isolate the reasons for that. Thus, they finally proposed a viable CPP radical-mediated mechanism involving the *in situ* generation of the CPP$\cdot$ species, together with C_2 as carbon source from the flow of ethanol. The latter mechanism would necessarily operate at high temperatures ($400 - 500$ C) to provide the homolytic C–H cleavage of the [n]CPPs. This experimental information clearly opens new possibilities for the growth mechanism and rates of SWCNT, and prompts for accurate and systematic theoretical studies exploring the role of the CPP$\cdot$ species.

Considering these experimental evidences, and the previous theoretical works as said before addressing the Diels-Alder[12] and the ethynyl radical addition mechanisms,[13,14] we will focus next on a mechanism involving the CPP$\cdot$ specie but substituting C_2 with acetylene C_2H_2 as carbon source (see sketch below).

Sketch: Reactants (left) and product (right) of the mechanism studied.

We will try to find out whether this mechanism could also be operative in practice, through a detailed mechanistic study using state-of-the-art (cost-effective and accurate) quantum-mechanical methods based on Density Functional Theory (DFT), and compare its energetics with other existing mechanisms also employing C_2H_2 as a carbon source. Note that, contrarily to previous studies, we will also address the influence of the underlying density functional expression, including some models (i.e. BMK or mPW1k) specifically derived for reaction kinetics as well as more sophisticated methods as double-hybrid density functionals (i.e. B2-PLYP). We will first explain the computational methods and technical details in Section 2, before passing to their benchmarking using some model system (Subsection 3.1) and to the corresponding extension to the set of [n]CPPs selected (Subsection 3.2).

2 Computational methods

For kinetic and mechanistic studies, larger-than-defaults EXact-like eXchange (EXX) weights are needed for accurate energy barrier heights.[15] It has been documented before that conventional density functionals (e.g. B3LYP) underestimate the reaction barrier heights[16] and/or might fail to locate the transition state for non-covalently bound complexes.[17] In order to control these flaws of common density functionals, we have thus selected a number of modern expressions ordered for their increasing EXX weights (in %), to

address the possible impact of this issue on thermochemistry and thermochemical kinetics of these systems: M06-L (0 %),[18] M06 (27 %),[18] BMK (42 %),[19] mPW1k (43 %),[20] M06-2X (54 %),[18] and M06-HF (100 %).[18] We have also added to the study the double-hybrid B2-PLYP method,[21] with a 53 % of EXX together with 27 % of MP2 correlation, to address the influence of going to higher orders of the hierarchy of DFT methods.[22] The 6-31G** and 6-311G** basis sets were initially used for studying basis set effects, and restricted (unrestricted) calculations were done for closed-shell (open-shell) species, with ultrafine grids always imposed for numerical integration.

The gas-phase Gibbs free energy of activation ($\Delta^{\ddagger}G$) and reaction ($\Delta_r G$) was calculated after locating and fully optimizing each transition state (reactants and products), verifying their nature by the presence (absence) of imaginary frequencies, and obtaining their zero-point energies correspondingly. The Berny algorithm,[23] as implemented in the Gaussian'09 package,[24] was used for that purpose with the regular convergence of forces lower than $4 \cdot 10^{-4}$ Hartree/Bohr. If not otherwise indicated, all calculations were performed at 1 atm and 298 K, with the energy of reactants taken as origin for Gibbs free energy profiles.

3 Results and discussion

3.1 Initial benchmarking of DFT methods

The large number of librational degrees of freedom existing in [n]CPPs (arising from the mutual orientation of neighbouring phenyl rings) precludes a brute-force procedure without selecting in advance the reaction sites. However, previous evidences show that the reaction mechanisms explored so far

(e.g. Diels-Alder) are highly local and occur in bay regions of the phenyl rings.[25,26] We will thus first proceed to benchmark the methodology using biphenyl as model system, taking advantage of its small size compared with the whole [n]CPP, and C_2H_2 as the other reactive agent. Using biphenyl as test case will allow us not only to try and discard different approaches to find the transition states that, in practice, is the hardest yet crucial part of the study, but also to bracket the $\Delta^{\ddagger}G$ and $\Delta_r G$ values according to the exchange-correlation functional choice, and to compare with previous estimates[14] although at a different temperature. We assume in the following that any evolution from reactants to products, passing through transition states, only depends on individual molecules; i.e., the growth would follow independent and continuous additions of C_2H_2 units. Figure 2 sketches the mechanism studied, showing the chemical structure of all the species involved as well as the notation followed to identify them.

Table 1 gathers the $\Delta^{\ddagger}G$ values for energy barrier heights to both transition states starting from the previous point on the energy diagram, that is $\Delta^{\ddagger}G$ (TS-1) = G(TS-1) − G(Reactants) and $\Delta^{\ddagger}G$ (TS-2) = G(TS-2) − G(Intermediate), with values roughly grouped in the 10–14 kcal/mol for $\Delta^{\ddagger}G$ (TS-1) and 3–6 kcal/mol for $\Delta^{\ddagger}G$ (TS-2). The dependence on the weight of the EXX introduced into the methods also emerges from the results, as it was expected, with the exception being the M06-L functional due to the parameterization strategy followed in that particular case.[27] To further confirm the underlying and marked dependence of the results on the EXX weight for hybrid density functionals, we now compare BMK (42 %) with mPW1k (43 %) and found differences as low as 0.2-0.3 kcal/mol for both $\Delta^{\ddagger}G$. Finally, we can see how the M06-2X and M06-HF results are the closest ones to the

benchmark B2-PLYP values, although the latter could also overlocalize electronic (spin)-densities in more extended systems due to the presence of a too high EXX weight.

Taking into account the following concomitant facts: (i) the marked dependence of the results on the density functional choice, and (ii) the importance of medium-range effects in the structure and energetics of barrier heights, we select for the rest of the study the M06-2X model. Note that this functional not only incorporates a high weight of EXX, actually similar to that of B2-PLYP, but it also deals efficiently with medium-range non-covalent interactions, which are expected to have some influence for nanorings of cyclic topology[11] and it may thus help to better locate transition states. Note also that this functional has shown to behave more accurately than other members of the M06 family of functionals in a wide assessment of structures and energies of excited states[28] while keeping a difference of roughly 2 kcal/mol with respect to predictions by BMK or mPW1k methods and only of 0.4 kcal/mol with respect to B2-PLYP. Actually, it has also been recently demonstrated to perform accurately for a wide variety of datasets for barrier heights,[29] and the use of this method would allow comparison with other modern mechanistic studies for cycloadditions of CPPs following Diels-Alder paths.[30] Concerning the still unexplored dependence of the results with the basis set size, we finally apply the M06-2X method with the larger 6-311G** basis set, to find values of the latter energies modified by only around 7 %, from 12.68 and 5.85 to 13.63 and 6.25 kcal/mol, respectively, and then to discard any pronounced basis sets effect with the smaller 6-31G**. Figure 3 finally shows the whole Gibbs free energy profile for both basis sets with this method of choice.

3.2 Extension to [n]CPPs

3.2.1 Viability of the initial step of the studied mechanism

We pioneeringly analyze first the energy penalties associated with the creation of the radicaloid species CPP· and C_2H·, that is, their bond dissociation energies defined as the standard enthalpy change when a bond is cleaved by homolysis, here in gas-phase and at 298 K, dubbed as DH_{298}:[31]

$$C_2H_2 \longrightarrow C_2H\cdot + H\cdot \quad (1)$$

$$[n]\text{CPP} \longrightarrow [n]\text{CPP}\cdot + H\cdot \quad (2)$$

Although these energies are notoriously difficult to measure, for some polyatomic systems like C_2H_2, or if we take the example of C_6H_6 for aromatic compounds, there are available experimental values[31] such as 133.3 ± 0.1 and 112.9 ± 0.5 kcal/mol, respectively, for C_2H· and C_6H_5·. Actually, we calculate DH_{298} values for the reactions sketched above at the M06-2X/6-31G** level, obtaining 131.5 and 111.4 kcal/mol, respectively, for C_2H· and [8]CPP· now. Note the reasonable agreement between experimental and calculated values for reaction (1), as well as the close values found between C_6H_6 or [n]CPP taken as reactants, which may be seen as another proof of the local nature of the mechanism studied. The theoretically calculated ratio $\frac{DH_{298}[\text{Reaction (2)}]}{DH_{298}[\text{Reaction (1)}]} \approx 1.2$ indicates the same or even slightly greater preference for the formation of the radical CPP· in presence of C_2H_2, and thus anticipating the dehydrogenation of [n]CPPs as energetically viable. Since the C_2H· radical could also be formed, specially at higher temperatures, we can not theoretically exclude a competition between both mechanisms, with this species acting as the initiator of both possible synthetic routes [n]CPP + C_2H· (after cleavage of C_2H_2) and [n]CPP· + C_2H_2 (after cleavage of [n]CPP) to be followed.

3.2.2 Dependence with diameter

The extension to the subset of [n]CPPs with n = 8, 10, and 12 will allow us to: (i) determine the viability of the corresponding CPP radical-activated mechanism (see Figure 4); (ii) assess its local nature (i.e. occurring at the bay region) comparing values employing biphenyl or [n]CPP; and (iii) find out its dependence with the system size (i.e. values of n). The Gibbs free energy profiles for the three cases considered (n = 8, 10, and 12) are presented in Figure 5, closely resembling actually the ones obtained before at the same theoretical level (M06-2X/6-31G**) for the simplified case of biphenyl. Table 1 also includes the values for both $\Delta^{\ddagger}G$ (TS-1) and $\Delta^{\ddagger}G$ (TS-2) magnitudes, slightly increasing (decreasing) with the system size and thus approaching the values for the reaction between biphenyl and C_2H_2 following the same mechanism. Figure 6 shows the evolution of the spin density for the species involved in the reaction mechanism, taking the case of [12]CPP as example, observing how it is localized at the reaction centers and smoothly evolves from reactants to products. The small variations observed with the size of molecules of $\Delta^{\ddagger}G$ (TS-1) with n might be related to the delocalization extent of the radicaloid CPP· involved as a function of the diameter, as it is theoretically[32] and experimentally found.[33,34] The slight decrease of $\Delta^{\ddagger}G$ (TS-2) may be rationalized by the partial release of the steric strain as n grows.

The values calculated for $\Delta^{\ddagger}G$ along this work can be only semi-quantitatively compared to previously calculated ones due to: (i) the use here of the M06-2X functional, more suited to mechanistic studies as indicated before compared with the B3LYP one,[35,36] and (ii) the temperature fixed here at 298K instead

of 450-500K. However, comparing with the Diels-Alder energy barrier heights for concave (inner face) or *endo* cycloadditions, the convex orientation is discouraged by steric reasons,[12] they range roughly between $55-65$ kcal/mol,[13] and thus we can infer a kinetic preference for this mechanism vs. the Diels-Alder cycloaddition in presence of same amounts of C_2H_2. Inspecting Figure 5 again, we remark how the reaction energy for the [8]CPP, [10]CPP, and [12]CPP remains nearly constant, actually between -51 and -53 kcal/mol, indicating also a large exothermicity, and favourable with respect to other mechanisms: the Diels-Alder cycloaddition is comprised between -44 and -47 kcal/mol, and the ethynyl radical reaction mechanism ranges approximately between -60 and -63 kcal/mol,[13] although these values calculated at the B3LYP/6-31G* level of theory.

3.2.3 Dependence with pressure and temperature

We finally consider the influence of pressure and temperature on the key thermodynamical magnitudes explored here, to assess their possible impact on the growth conditions. Figure 7 shows the changes in Gibbs free energy of activation ($\Delta^{\ddagger}G$) and reaction ($\Delta_r G$) at different temperatures and at P = 1 atm. A higher pressure of 10 atm altered the values by less than 5 %, and will not be thus discussed further. Whereas $\Delta^{\ddagger}G$ (TS-1) increases with temperature, $\Delta^{\ddagger}G$ (TS-2) remains almost unchanged due to its intramolecular character, and thus without significant entropy contributions. The values of $\Delta_r G$ are comprised between -52 (273K) and -34 kcal/mol (673K), indicating overall a slight preference for room conditions.

4 Conclusions

We have reported the energetics of a mechanism for the growth of SWCNT using [n]CPP· and C_2H_2 as organic precursors, with the former molecule acting as template and driving the stereoregularity of the reaction at the bay regions in which the initial dehydrogenation takes place. In order to exclude any influence of the exchange-correlation functional choice on the results, we have systematically assessed the performance of different models for thermochemical kinetics using a cost-effective system (i.e. substituting [n]CPP by biphenyl) which have further helped us to confirm the negligible dependence of the [n]CPP diameter on the final results, contrarily to what happens in other mechanisms formerly explored at the theoretical level. Actually, despite the possible competition between the ethynyl mediated mechanism, involving [n]CPP and C_2H· as reactants, and the one evaluated here, with [n]CPP· and C_2H_2, we confirm that the latter mechanism could also operate in practice due to the trace amounts at which C_2H· is found in experimental growth conditions. The [n]CPP· radical regenerates at the end of the process, which may favour the endless addition of C_2H_2 units in ideal conditions. In summary, through this study, We aim at providing valuable insights to motivate further experimental and theoretical studies towards the envisioned synthesis of SWCNT in a fully controlled manner.

Acknowledgements

We acknowledge the "Ministerio de Economía y Competitividad" of Spain and the "European Regional Development Fund" through project CTQ2014-55073-P.

References

[1] De Volder, M. F.; Tawfick, S. H.; Baughman, R. H.; Hart, A. J. Carbon Nanotubes: Present and Future Commercial Applications. *Science* **2013**, *339*, 535–539.

[2] Iijima, S. Helical Microtubules of Graphitic Carbon. *Nature* **1991**, *354*, 56.

[3] Guo, T.; Nikolaev, P.; Thess, A.; Colbert, D. T.; Smalley, R. E. Catalytic Growth of Single-walled Nanotubes by Laser Vaporization. *Chemical Physics Letters* **1995**, *243*, 49–54.

[4] Yacamán, M. J.; ; Miki-Yoshida, M.; Rendón, L.; Santiesteban, J. Catalytic Growth of Carbon Microtubules with Fullerene Structure. *Applied Physics Letters* **1993**, *62*, 657–659.

[5] Omachi, H.; Segawa, Y.; Itami, K. Synthesis of Cycloparaphenylenes and Related Carbon Nanorings: A Step Toward the Controlled Synthesis of Carbon Nanotubes. *Accounts of Chemical Research* **2012**, *45*, 1378–1389.

[6] Segawa, Y.; Yagi, A.; Itami, K. Chemical Synthesis of Cycloparaphenylenes. *Physical Sciences Reviews* **2017**, *2*.

[7] Zhang, F.; Hou, P.-X.; Liu, C.; Cheng, H.-M. Epitaxial Growth of Single-wall Carbon Nanotubes. *Carbon* **2016**, *102*, 181–197.

[8] Golder, M. R.; Jasti, R. Syntheses of the Smallest Carbon Nanohoops and the Emergence of Unique Physical Phenomena. *Accounts of Chemical Research* **2015**, *48*, 557–566.

[9] Golder, M. R.; Colwell, C. E.; Wong, B. M.; Zakharov, L. N.; Zhen, J.; Jasti, R. Iterative Reductive Aromatization/Ring-Closing Metathesis Strategy toward the Synthesis of Strained Aromatic Belts. *Journal of the American Chemical Society* **2016**, *138*, 6577–6582.

[10] Omachi, H.; Nakayama, T.; Takahashi, E.; Segawa, Y.; Itami, K. Initiation of Carbon Nanotube Growth by Well-defined Carbon Nanorings. *Nature Chemistry* **2013**, *5*, 572–576.

[11] Climent-Medina, J.-V.; Pérez-Jiménez, Á.-J.; Moral, M.; San-Fabián, E.; Sancho-García, J.-C. Intra-and Intermolecular Dispersion Interactions in [n]Cycloparaphenylenes: Do They Influence Their Structural and Electronic Properties? *ChemPhysChem* **2015**, *16*, 1520–1528.

[12] Fort, E. H.; Scott, L. T. Carbon Nanotubes from Short Hydrocarbon Templates. Energy Analysis of the Diels–Alder Cycloaddition/Rearomatization Growth Strategy. *Journal of Materials Chemistry* **2011**, *21*, 1373–1381.

[13] Li, H.-B.; Page, A. J.; Irle, S.; Morokuma, K. Single-walled Carbon Nanotube Growth from Chiral Carbon Nanorings: Prediction of Chirality and Diameter Influence on Growth Rates. *Journal of the American Chemical Society* **2012**, *134*, 15887–15896.

[14] Li, H.-B.; Page, A. J.; Irle, S.; Morokuma, K. Theoretical Insights into Chirality-Controlled SWCNT Growth from a Cycloparaphenylene Template. *ChemPhysChem* **2012**, *13*, 1479–1485.

[15] Zhao, Y.; Truhlar, D. G. Hybrid Meta Density Functional Theory Methods for Thermochemistry, Thermochemical Kinetics, and Noncovalent Interactions: the MPW1B95 and MPWB1K Models and Comparative

Assessments for Hydrogen Bonding and van der Waals Interactions. *The Journal of Physical Chemistry A* **2004**, *108*, 6908–6918.

[16] Lynch, B. J.; Truhlar, D. G. How well can hybrid density functional methods predict transition state geometries and barrier heights? *The Journal of Physical Chemistry A* **2001**, *105*, 2936–2941.

[17] Su, N. Q.; Xu, X. Beyond energies: geometry predictions with the XYG3 type of doubly hybrid density functionals. *Chemical Communications* **2016**, *52*, 13840–13860.

[18] Zhao, Y.; Truhlar, D. G. The M06 Suite of Density Functionals for Main Group Thermochemistry, Thermochemical Kinetics, Noncovalent Interactions, Excited States, and Transition Elements: Two New Functionals and Systematic Testing of Four M06-class Functionals and 12 Other Functionals. *Theoretical Chemistry Accounts: Theory, Computation, and Modeling (Theoretica Chimica Acta)* **2008**, *120*, 215–241.

[19] Boese, A. D.; Martin, J. M. Development of Density Functionals for Thermochemical Kinetics. *The Journal of Chemical Physics* **2004**, *121*, 3405–3416.

[20] Lynch, B. J.; Fast, P. L.; Harris, M.; Truhlar, D. G. Adiabatic connection for kinetics. *The Journal of Physical Chemistry A* **2000**, *104*, 4811–4815.

[21] Grimme, S. Semiempirical Hybrid Density Functional with Perturbative Second-Order Correlation. *The Journal of Chemical Physics* **2006**, *124*, 034108.

[22] Bremond, E.; Ciofini, I.; Sancho-García, J. C.; Adamo, C. Nonempirical double-hybrid functionals: An effective tool for chemists. *Accounts of Chemical Research* **2016**, *49*, 1503–1513.

[23] Berny, A. *Theoretical Aspects of Evolutionary Computing*; Springer, 2001; pp 287–306.

[24] Frisch, M. J. et al. Gaussian 09 Revision E.01. Gaussian Inc. Wallingford CT 2009.

[25] Fort, E. H.; Donovan, P. M.; Scott, L. T. Diels- Alder Reactivity of Polycyclic Aromatic Hydrocarbon Bay Regions: Implications for Metal-Free Growth of Single-Chirality Carbon Nanotubes. *Journal of the American Chemical Society* **2009**, *131*, 16006–16007.

[26] Jackson, E. P.; Sisto, T. J.; Darzi, E. R.; Jasti, R. Probing Diels–Alder Reactivity on a Model CNT Sidewall. *Tetrahedron* **2016**, *72*, 3754–3758.

[27] Zhao, Y.; Truhlar, D. G. A New Local Density Functional for Main-group Thermochemistry, Transition Metal Bonding, Thermochemical Kinetics, and Noncovalent Interactions. *The Journal of Chemical Physics* **2006**, *125*, 194101.

[28] Su, N. Q.; Pernot, P.; Xu, X.; Savin, A. When does a functional correctly describe both the structure and the energy of the transition state? *Journal of Molecular Modeling* **2017**, *23*, 65.

[29] Mardirossian, N.; Head-Gordon, M. How Accurate Are the Minnesota Density Functionals for Noncovalent Interactions, Isomerization Energies, Thermochemistry, and Barrier Heights Involving Molecules Composed of Main-Group Elements? *Journal of Chemical Theory and Computation* **2016**, *12*, 4303–4325.

[30] Dang, J.; Wang, W.; Zhao, X.; Nagase, S. Mechanistic Study on Cationic Li Prompted Diels-Alder Cycloaddition of Cycloparaphenylene. *Organic Chemistry Frontiers* **2017**, *4*, 1757–1761.

[31] Blanksby, S. J.; Ellison, G. B. Bond Dissociation Energies of Organic Molecules. *Accounts of Chemical Research* **2003**, *36*, 255–263.

[32] Sancho-Garcia, J.-C.; Moral, M.; Pérez-Jiménez, A. Effect of Cyclic Topology on Charge-transfer Properties of Organic Molecular Semiconductors: The Case of Cycloparaphenylene Molecules. *The Journal of Physical Chemistry C* **2016**, *120*, 9104–9111.

[33] Kayahara, E.; Kouyama, T.; Kato, T.; Takaya, H.; Yasuda, N.; Yamago, S. Isolation and Characterization of the Cycloparaphenylene Radical Cation and Dication. *Angewandte Chemie International Edition* **2013**, *52*, 13722–13726.

[34] Kayahara, E.; Kouyama, T.; Kato, T.; Yamago, S. Synthesis and Characterization of [n]CPP (n = 5, 6, 8, 10, and 12) Radical Cation and Dications: Size-Dependent Absorption, Spin, and Charge Delocalization. *Journal of the American Chemical Society* **2016**, *138*, 338.

[35] Becke, A. D. Density-Functional Thermochemistry. III. The Role of Exact Exchange. *The Journal of Chemical Physics* **1993**, *98*, 5648–5652.

[36] Barone, V.; Adamo, C. Theoretical Study of Direct and Water-assisted Isomerization of Formaldehyde Radical Cation. A Comparison Between Density Functional and Post-Hartree-Fock Approaches. *Chemical Physics Letters* **1994**, *224*, 432–438.

- **Table 1.** Upper: Comparison between $\Delta^{\ddagger}G$ values (kcal/mol) for both transition states involved in the biphenyl and C_2H_2 radical-mediated mechanism, as a function of the functional choice and with the 6-31G** basis set. Lower: Comparison between $\Delta^{\ddagger}G$ values (kcal/mol) for both transition states involved in the $[n]$CPP and C_2H_2 radical-mediated mechanism, as a function of the $[n]$CPP size and at the M06-2X/6-31G** level.

Table 1:

Reactants	Functional	$\Delta^{\ddagger}G$ (TS-1)	$\Delta^{\ddagger}G$ (TS-2)
Biphenyl + C_2H_2	M06-L	11.36	3.36
	M06	10.37	3.52
	BMK	14.14	3.55
	mPW1k	14.04	3.22
	M06-2X	12.68	5.85
	M06-HF	13.07	6.15
	B2-PLYP	13.11	6.22
[8]CPP + C_2H_2	M06-2X	10.34	10.97
[10]CPP + C_2H_2	M06-2X	11.16	10.04
[12]CPP + C_2H_2	M06-2X	11.32	9.41

- **Figure 1.** Chemical structures of the [n]CPP systems.

- **Figure 2.** Sketch of the radical-mediated mechanism studied, employing biphenyl and C_2H_2 as reactants (TS indicates the transition state found).

- **Figure 3.** Gibbs free energy profile for the radical-mediated mechanism studied, employing biphenyl and C_2H_2 as reactants, with the M06-2X functional and the 6-31G** and 6-311G** basis sets.

- **Figure 4.** Sketch of the radical-mediated mechanism studied, employing [n]CPP and C_2H_2 as reactants (TS indicates the transition state found).

- **Figure 5.** Gibbs free energy profile for the radical-mediated mechanism studied, employing [n]CPPs and C_2H_2 as reactants, at the M06-2X/6-31G** level.

- **Figure 6.** Isocontour plots (0.005 e/bohr^3) of the spin-density for the radical-mediated mechanism studied.

- **Figure 7.** Evolution of Gibbs free energy reaction and barrier heights with temperature, for the [8]CPP case, at the M06-2X/6-31G** level.

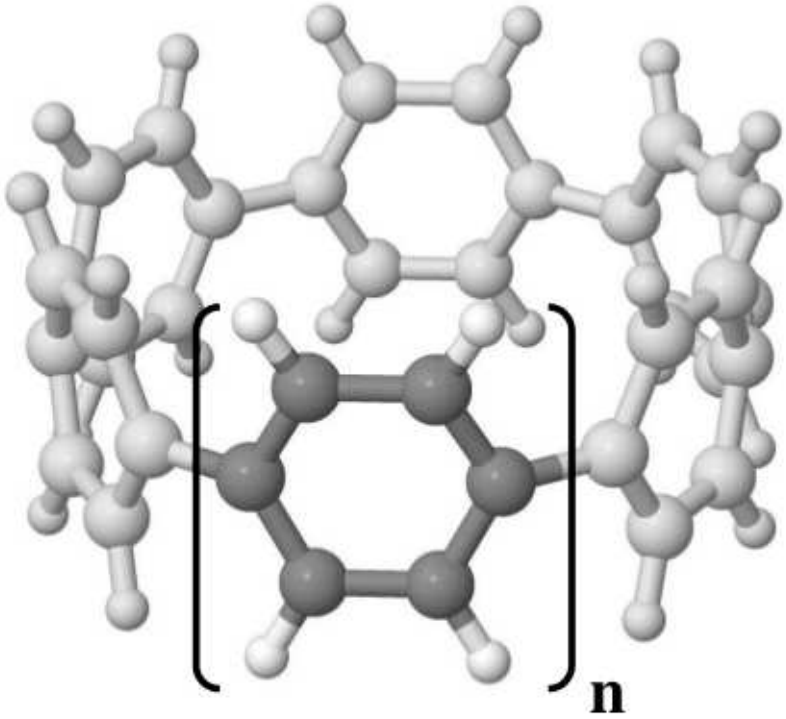

Figure 1.

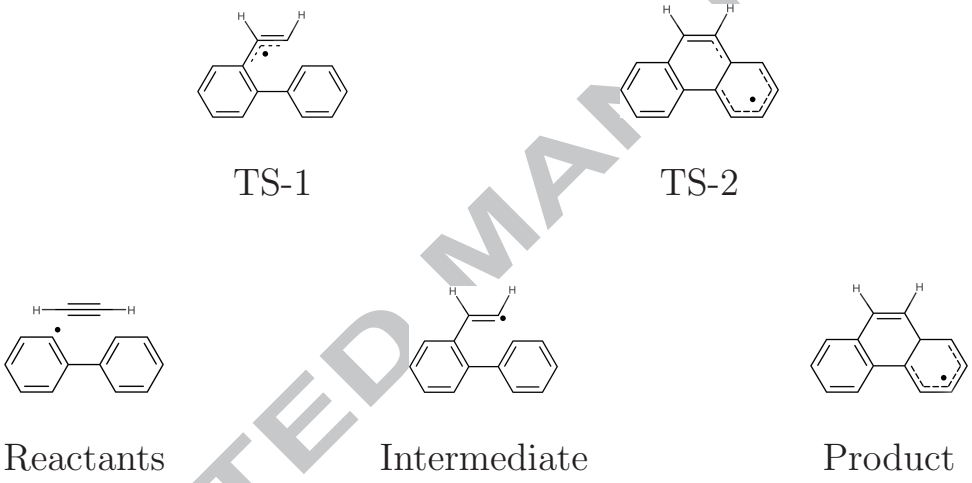

Figure 2.

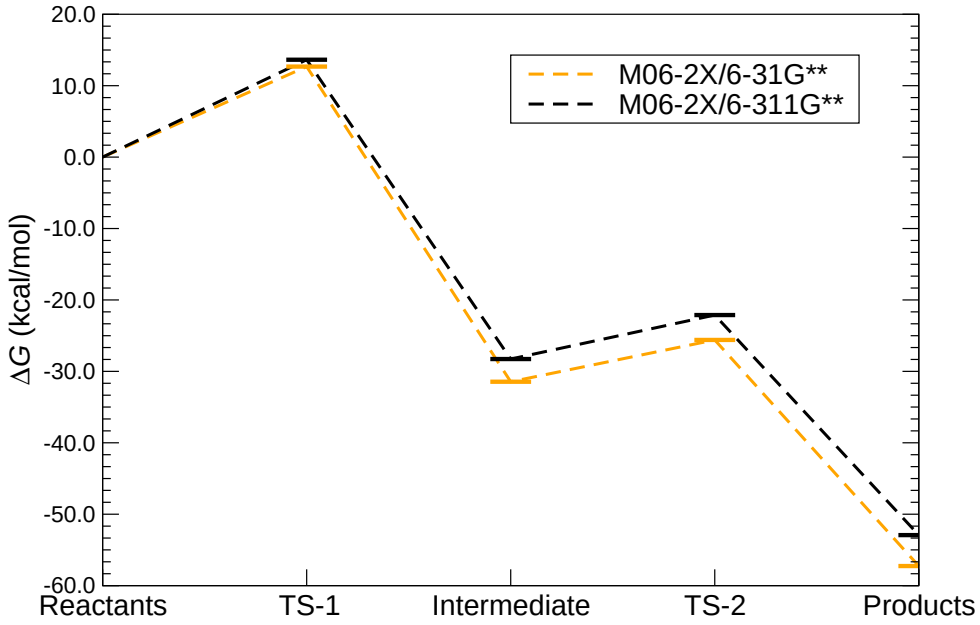

Figure 3.

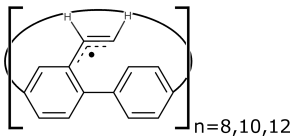

TS-1

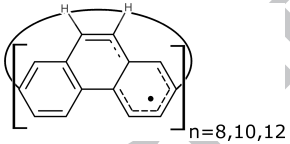

TS-2

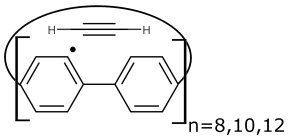

Reactants

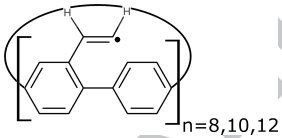

Intermediate

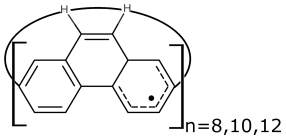

Product

Figure 4.

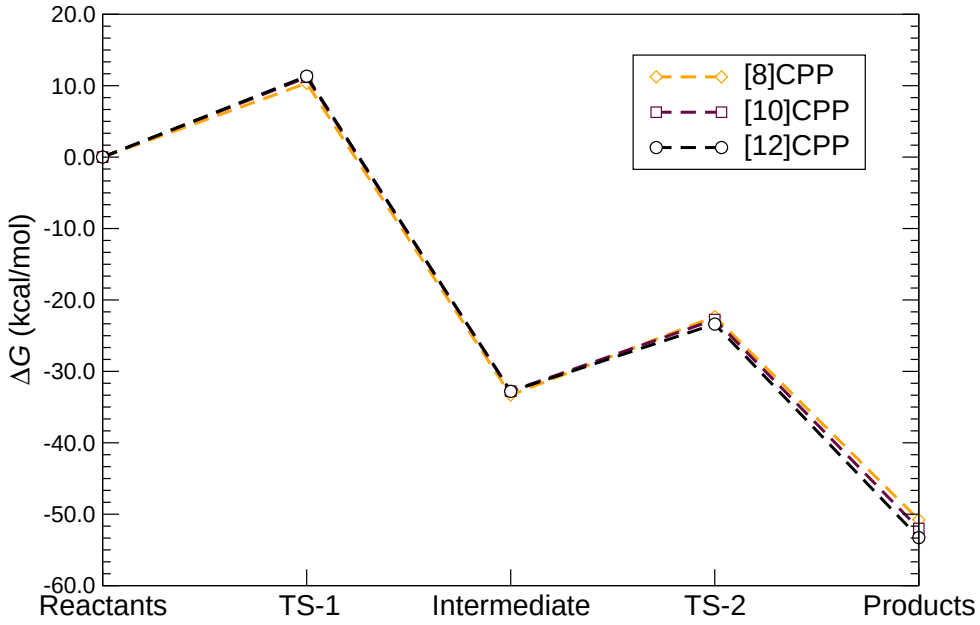

Figure 5.

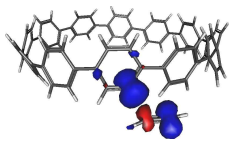

TS-1

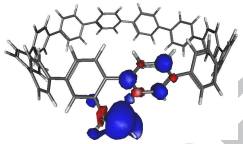

TS-2

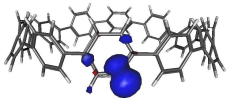

Reactants

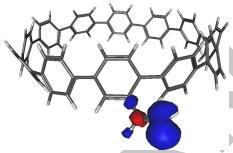

Intermediate

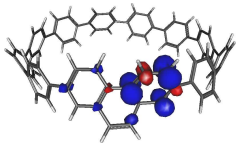

Product

Figure 6.

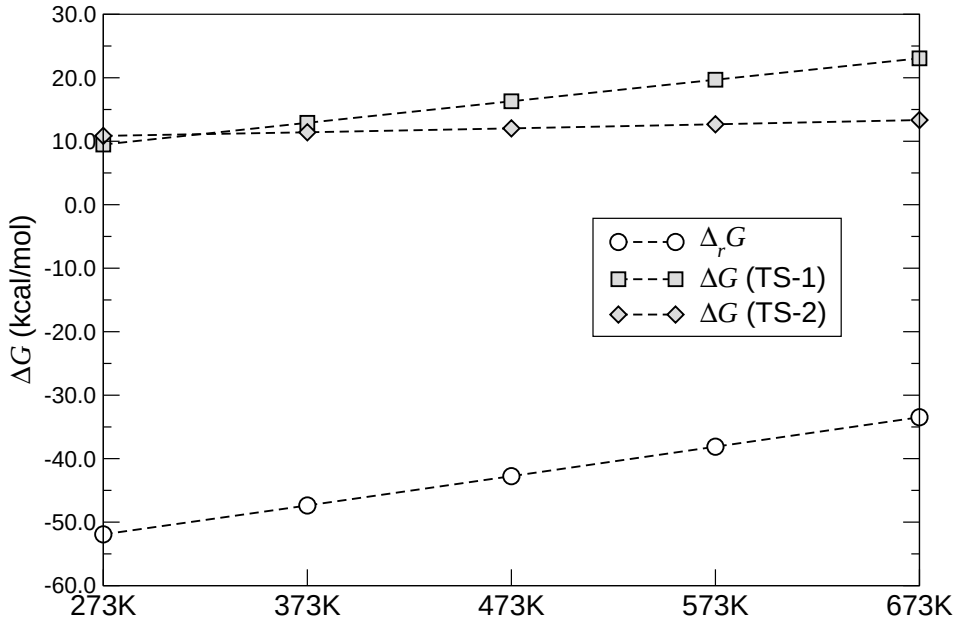

Figure 7.

Research Highlights

1) We study the possible growth of carbon nanotubes through a radical-mediated mechanism

2) The studied mechanism involves CPP· and C_2H_2 species as reactants

3) We apply a set of selected state-of-the-art DFT functionals

4) The dependence of the mechanism with the diameter of the nanoring is also investigated

Graphical Abstract

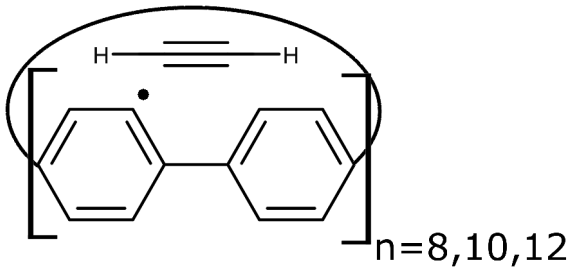

A radical-mediated mechanism is proposed involving cyclic phenylenes and C_2H_2 as a carbon source, to investigate the growth of CNTs from these precursors.